# Raman response of stage-1 graphite intercalation compounds revisited

J. C. Chacón-Torres,[1,*] A. Y. Ganin,[2] M. J. Rosseinsky,[2] and T. Pichler[1,†]
[1]*Faculty of Physics, University of Vienna, Strudlhofgasse 4, A-1090 Vienna, Austria*
[2]*Department of Chemistry, University of Liverpool, Liverpool L69 7ZD, United Kingdom*
(Received 27 April 2012; published 2 August 2012)

We present a detailed *in situ* Raman analysis of stage-1 $KC_8$, $CaC_6$, and $LiC_6$ graphite intercalation compounds to unravel their intrinsic fingerprint. Four main components were found between 1200 $cm^{-1}$ and 1700 $cm^{-1}$ and each of them were assigned to a corresponding vibrational mode. From a detailed line-shape analysis of the intrinsic Fano lines of the *G*- and *D*-line response we precisely determine the position ($\omega_{ph}$), line width ($\Gamma_{ph}$), and asymmetry ($q$) from each component. The comparison to the theoretical calculated line width and position of each component allows us to extract the electron-phonon coupling constant of these compounds. A coupling constant $\lambda_{ph} < 0.06$ was obtained. This highlights that Raman active modes alone are not sufficient to explain the superconductivity within the electron-phonon coupling mechanism in $CaC_6$ and $KC_8$.

DOI: 10.1103/PhysRevB.86.075406 PACS number(s): 74.25.nd, 74.70.Wz

## I. INTRODUCTION

$Sp^2$ hybridized carbon allotropes have unique structural properties in different dimensions such as graphite [three-dimensional (3D)], graphene (2D), single-walled carbon nanotubes (1D), and fullerene molecules ("quasi-0D"). They have been widely studied due to their interesting electronic properties ranging from metallic, semimetallic, (zero-gap) semiconducting to wide-gap semiconducting, and insulating.[1–4] One unique possibility to tailor their electronic properties is by intercalation of alkali and alkaline-earth ions. These intercalation compounds are particularly appealing for their application in batteries and because of their superconducting phases. Superconductivity, as a result of alkali-metal intercalation, was first studied by Henning[5] in graphite intercalation compounds (GICs) and further studies.[6,7] However, until 1981, the critical temperature ($T_c$) in stage-1 $XC_8$ GICs ($X$ = K, Rb, and Cs) reported was low,[1] not higher than 0.135 K for $CsC_8$, and between 0.39–0.55 K for $KC_8$. This is surprising since GICs are BCS superconductors based on electron-phonon coupling owing to an exceptionally high electron-phonon coupling constant up to $\lambda = 0.45$ in the case of $KC_8$ and high phonon frequency of the optical modes.[8] For instance, using $\lambda = 0.45$ and a phonon frequency of 1337 $cm^{-1}$ a BCS $T_c$ of ∼5 K would be possible in $KC_8$, which is much higher than the observed $T_c$ up to 0.55 K, and this can be related to a screened Coulomb pseudopotential of $\mu^* = 0.14$, which is on the lower bound with respect to $CaC_6$.[9]

The discovery of fullerene intercalation compounds, so-called fullerides, added a new family of organic superconductors of type $A_3C_{60}$ ($A$ = alkali-metal).[10–12] Compared to classical superconductors, and in contrast to GICs the $T_c$ observed in fullerides is high, ranging from 18 K for $K_3C_{60}$, 28 K for $Rb_3C_{60}$, up to 39 K for $Cs_3C_{60}$.[11–13] Contrary to GICs, where the highest intercalation level represents the superconducting phase, for fullerides the superconducting phase is a line phase at half filling. Other stable fullerides $A_1C_{60}$, $A_4C_{60}$ and $A_6C_{60}$ are either normal metals, Mott-Hubbard insulators, or charge transfer insulators.[14] Similar to GICs the superconducting coupling mechanism was described within the framework of BCS theory involving an electron-phonon coupling to the intramolecular modes of $C_{60}$.[3] Experimentally, most important for the coupling are the two low-energy intramolecular modes with $H_g$ symmetry,[15,16] although theoretically the high-frequency phonons have been predicted to play a significant role.[17,18]

For GICs, the observation of superconductivity of $CaC_6$ with a high $T_c$ of[19] 11.5 K triggered further research in the field and led to alternative explanations of the superconducting electron-phonon coupling. For instance, Kim *et al*. attribute superconductivity in $CaC_6$ to the high-energy C modes.[20] Hinks *et al*.[21] report that the low-energy modes of the intercalant were responsible for superconductivity inferred from specific heat analysis, while first-principle calculations predict equal coupling to both groups of phonons.[9,22] Therefore, the exact contribution of the different coupling phonons still remain elusive.

Raman spectroscopy became then an important tool to determine the exact contribution of each phonon, and it opened a route for revealing the coupling mechanism in superconducting fullerides and GICs. Hence, it serves as a key tool to analyze the electron-phonon coupling constant ($\lambda$) from a renormalization of the optical response of the intramolecular $C_{60}$ modes and of the graphitic *G*-line response. Recent Raman studies on the *G*-line response of different stage-1 GICs reported the assignment of the electron-phonon coupling (EPC) induced line width $\gamma^{EPC}$ to the 1510 $cm^{-1}$ mode,[23–26] which has been explained by the inclusion of nonadiabatic phonon calculations.[24,26] However, the intrinsic *G*-line response in heavily doped graphite compounds is still elusive because of the influence of defects and laser-induced deintercalation, as recently reported using a micro-Raman analysis for[24] $CaC_6$ and for $KC_8$ single crystals.[27]

In this contribution we report a detailed study of the *D* and *G* lines in $KC_8$, $CaC_6$, and $LiC_6$ GICs, in order to unravel their intrinsic phonon components and their relation to the electron-phonon coupling constant responsible for superconductivity. From the analysis of the optical phonons observed, we assign their role in the superconductivity coupling mechanism in comparison with previous results of electron-doped GICs.

## II. EXPERIMENT AND MEASUREMENT DETAILS

The synthesis of $KC_8$ was performed *in situ* under high vacuum (∼ $4 \times 10^{-8}$ mbar) conditions in a quartz tube with

 

natural graphite flake single crystals from different sources, and a potassium ingot with 99.95% purity (Aldrich) for the intercalation. Potassium was evaporated until golden crystals were obtained. This phase can be directly assigned to stage-1 $KC_8$ phase from a comparison of the Raman response with previous combined Raman and XRD results.[27,28] $CaC_6$, and $LiC_6$ were prepared in a sealed ampoule by using a procedure described elsewhere.[29] Highly oriented pyrolytic graphite (HOPG) flakes were degassed and used for lithium and calcium intercalation for ten days under He atmosphere (ca. 0.5 atm). The ampoule was then opened in the glove box and gold colored product was extracted from the melt. Powder x-ray diffraction measurements were carried out using a Stadi-P diffractometer ($CuK_a$) to confirm the intercalation stage in $CaC_6$ and $LiC_6$. For the Raman analysis every GIC was kept in vacuum ($\sim 4 \times 10^{-8}$ mbar) in order to avoid deintercalation due to exposure to air. The Raman analysis was performed with a HORIBA LabRam at room temperature, with a 568-nm wavelength, and 0.25 mW of laser power. Every spectrum was acquired under the same conditions in a range from 500 $cm^{-1}$ up to 2500 $cm^{-1}$ and the line positions were calibrated by gauge lamps.

## III. RESULTS AND DISCUSSION

In the Raman response of stage-1 GICs eight optical vibrational modes are present[28] in the following irreducible representation:

$$\Gamma = 2A_{2u} + 2B_{2g} + 2E_{1u} + 2E_{2g}.$$

The $E_{2_{g_1}}$ and the $E_{2_{g_2}}$ vibrational modes are Raman active, and the $A_{2u}$ and $E_{1u}$ belong to infrared active modes.[1,30] There are some other modes in graphite that are forbidden in perfect graphite and only become active in the presence of disorder, such as the mode with $A_{1g}$ symmetry. In Fig. 1(a), the optical modes of graphite are depicted. Previous Raman studies in GICs have confirmed the presence of the $E_{2g}$ mode around 1600 $cm^{-1}$, the $A_{2u}$ ($c$-axis mode) around 500 $cm^{-1}$, and the absence of the $A_{1g}$[1,28]. The $c$-axis mode has been attributed to an out-of-plane C motion in graphite.[24] This mode correspond to the **M** point of the graphene Brillouin zone and it becomes Raman active when high intercalation levels are achieved. In agreement with the literature, we observe [as shown in in Fig.1(b)], that the $c$-axis mode is present solely in $KC_8$ around ~560 $cm^{-1}$. Surprisingly and in agreement with previous studies neither in $CaC_6$, nor in $LiC_6$ is this mode observed.[23,31]

Regarding the $G$-line response all these previous studies reported one $G$ line, which has a strong Fano line shape due to the coupling and the interference with the conduction electrons. Taking a closer look on the line shape of the $G$-line response in Fig. 1(b), one can easily see that more than one component is present and a detailed line-shape analysis is needed in order to unravel their intrinsic response and related electron-phonon coupling of these stage-1 GICs. The line-shape analysis of the $G$ line is discussed in detail below.

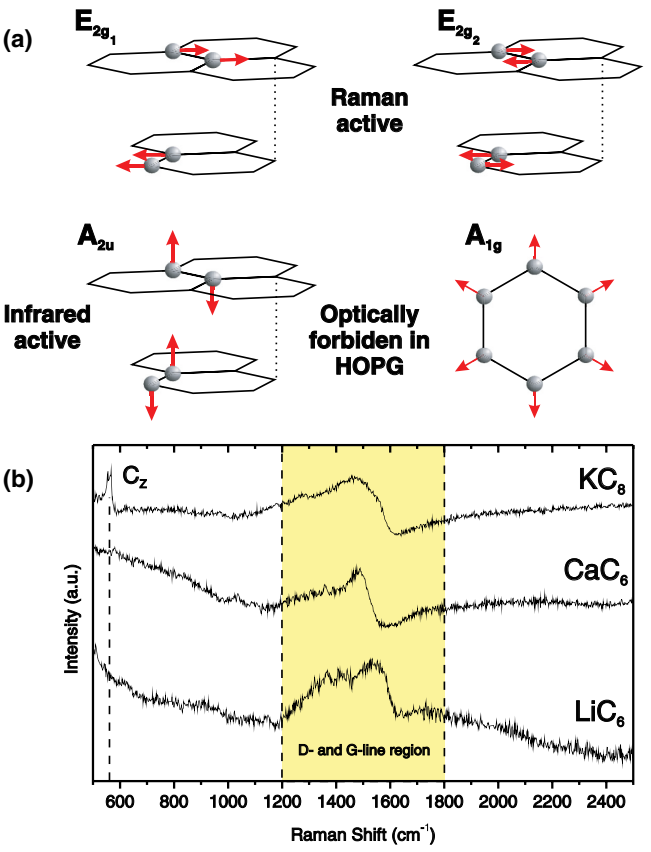


FIG. 1. (Color online) (a) Optical modes of graphite. (b) Raman spectra from $KC_8$, $CaC_6$, and $LiC_6$ taken with 568-nm laser at room temperature and low laser power of 0.25 mW.

### A. Analysis of the intrinsic $G$-line response of stage-1 graphite intercalation compounds

The structure of the intercalation stages in graphitic compounds has been studied and it is well understood from x-ray diffraction.[28] However, the intrinsic Raman response of stage-1 GICs is still complicated by laser-induced deintercalation from a local heating of the sample with different laser power densities.[30] In addition, other factors such as 3D intrinsic disorder of the crystal also strongly affect the Raman response in GICs. For example, a graphite single crystal doped to stage 1 will remain polycrystalline due to a nonhomogeneous intercalation. This will limit the achievable doping in these GICs.[24,32]

Hence, the previous experimental and theoretical results on the Raman response of $KC_8$ and $CaC_6$ reported in the literature are not conclusive with respect to the $G$-line shape and position. In different studies a wide range of different $G$-line positions between ~1400 $cm^{-1}$ and ~1600 $cm^{-1}$ are reported (i.e., at ~1500 $cm^{-1}$[11], between 1400 $cm^{-1}$ and 1550 $cm^{-1}$[28], 1534 $cm^{-1}$[26], 1547 $cm^{-1}$[30], 1420 $cm^{-1}$, and 1582 $cm^{-1}$).[33] In more recent experiments for calcium GICs,[24,25] potassium-doped graphene and graphite,[27,32] and later in Li graphite,[31] the strongest $G$-line phonon response is observed around 1510 $cm^{-1}$ when the sample has the best quality (lowest defect content) and highest intercalation.

In Fig. 2(a) the $D$- to $G$-band region of pristine stage-1 intercalation compounds with K, Ca, and Li is depicted and

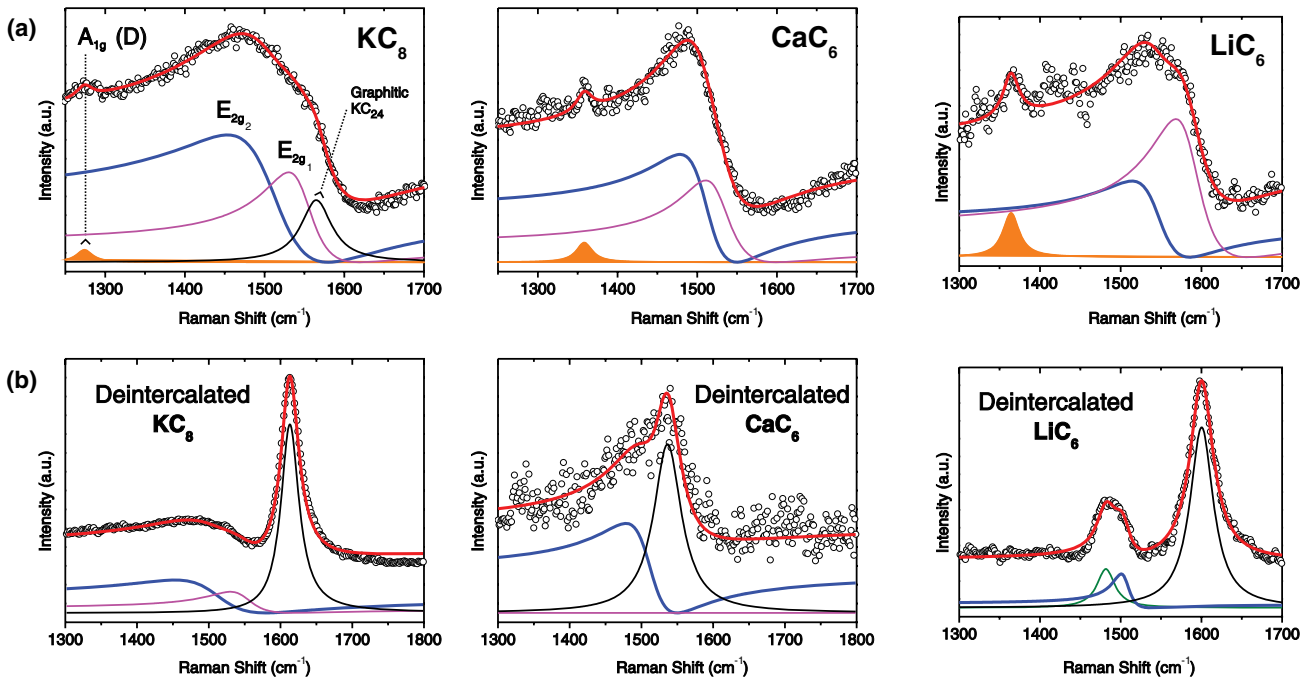


FIG. 2. (Color online) $D$- and $G$-line analysis for stage-1 GICs and Raman response of their laser-induced deintercalated phases. The four components that can be identified in the $G$-line shape are: $\mathbf{A}_{1g}$ mode between 1250 and 1350 cm$^{-1}$, $\mathbf{E}_{2g_2}$ mode ∼1510 cm$^{-1}$, $\mathbf{E}_{2g_1}$ mode at ∼1547 cm$^{-1}$, and stage-2 $G$ mode ∼1560 cm$^{-1}$. In the upper panel (a) we can observe that $KC_8$ exhibits a strong contribution from the $\mathbf{E}_{2g_2}$ with a broad Fano behavior, which is the fingerprint for the intrinsic line of a stage-1 compound.[27] In the lower panel (b) we present the same crystals analyzed in the upper panel but deintercalated. We can clearly observe the decrease of the $\mathbf{E}_{2g_2}$ mode, concomitant to a strong increase of the $G$ mode assigned to the $XC_{24}$ graphitic face ∼1600 cm$^{-1}$.

clearly shows the presence of shoulders in the response, which indicate different components. Nevertheless, in order to compare with the previous studies[26,30,33] we first conducted a line-shape analysis of the $G$ line by using a single Breit-Wigner-Fano (BWF) function. This yields parameters that are in good agreement to those results, and confirms that our samples have the same high quality of a true stage-1 compound. This is further supported by the fact that the $G$ line assigned to stage-2 compounds around 1600 cm$^{-1}$ is only increased upon (e.g., laser-induced de-intercalation [see Fig. 2(b)]).

In a second step a detailed and accurate analysis of the line shape in the $D$- to $G$-band region of these GICs was conducted using four components. The assignment of each component to the $A_{1g}(D)$, $E_{2g_2}$, $E_{2g_1}$ modes, and the $G$ line of the stage-2 compound is explained in the following.

Regarding the line shape, all components have been fitted using BWF functions of the form

$$I(w) = I_0 \frac{\left(1+\frac{w-w_{\rm ph}}{q\,\Gamma/2}\right)^2}{1+\left(\frac{w-w_{\rm ph}}{\Gamma/2}\right)^2} + A,$$

where $\omega_{\rm ph}$ is the phonon frequency, $\Gamma$ the line width or damping, $\mathbf{q}$ the asymmetry parameter, and $A$ an offset. For the first and fourth peak ($D$ and $G$), the asymmetry was $\mathbf{q} = 10^5$ approaching a Lorentzian function, while the second and third (split $G$ line) have a pronounced Fano interference. In the analysis, in order to get comparable results for each GIC, the same values of $\Gamma$ and $\mathbf{q}$ were used to fit each respective component. The parameters are summarized in Table I together with the calculated values from the adiabatic and nonadiabatic phonons from Ref. 26.

The first mode observed in Fig. 2(a) between 1260 and 1360 cm$^{-1}$ has been previously attributed to particle size effects and/or the presence of disorder.[34,35] It has been assigned to the $A_{1g}$ vibration, which is forbidden in perfect graphite. Therefore, this mode is called $D$ line (intrinsic "defect mediated"), and it involves the contribution from the phonons near the $K$ zone boundary with a Lorentzian line shape.

TABLE I. Fit parameters to the four components of the $D$ and $G$ line in the Raman spectra of $KC_8$, $CaC_6$, and $LiC_6$.

| $KC_8$ | $\omega_{\rm ph}(cm^{-1})$ | $\Gamma_{\rm ph}(cm^{-1})$ | q | $\omega_A$[a] | $\omega_{NA}$[b] |
|---|---|---|---|---|---|
| **D** | 1274 | 24.3 | $10^5$ | – | – |
| $E_{2g_2}$ | 1510 | 125.6 | −1.09 | 1223 | 1534 |
| $E_{2g_1}$ | 1547 | 70.9 | −2.02 | 1223 | 1534 |
| **G**[c] | 1565 | 47.0 | $10^5$ | – | – |
| $CaC_6$ | $\omega_{\rm ph}(cm^{-1})$ | $\Gamma_{\rm ph}(cm^{-1})$ | q | $\omega_A$[a] | $\omega_{NA}$[b] |
| **D** | 1358 | 24.3 | $10^5$ | – | – |
| $E_{2g_2}$ | 1510 | 71.0 | −1.09 | 1446 | 1529 |
| $E_{2g_1}$ | 1528 | 70.9 | −2.02 | 1446 | 1529 |
| $LiC_6$ | $\omega_{\rm ph}(cm^{-1})$ | $\Gamma_{\rm ph}(cm^{-1})$ | q | $\omega_A$[a] | $\omega_{NA}$[b] |
| **D** | 1364 | 24.3 | $10^5$ | – | – |
| $E_{2g_2}$ | 1546 | 71.0 | −1.09 | 1362 | 1580 |
| $E_{2g_1}$ | 1585 | 70.9 | −2.02 | 1362 | 1580 |

[a]Calculated adiabatic $E_{2g}$ phonon frequencies (Ref. 26) in cm$^{-1}$.
[b]Calculated nonadiabatic $E_{2g}$ phonon frequencies (Ref. 26) in cm$^{-1}$.
[c]$G$-line contribution from $KC_{24}$ stage-2 compound.

The second and third modes observed are assigned to the $E_{2g}$ graphitic mode of heavily doped graphene layers [Fig. 2(a)]. Both components have a pronounced asymmetry and they are well described by a BWF line shape. We label the two modes as $E_{2g_1}$ and $E_{2g_2}$. The $E_{2g_1}$ mode is located between 1528 $cm^{-1}$ and 1585 $cm^{-1}$ and it is attributed to not homogeneous or incomplete intercalation in stage-1 compounds.[27] The $E_{2g_2}$ mode locates at 1510 $cm^{-1}$ for $KC_8$ and $CaC_6$, and 1546 $cm^{-1}$ for $LiC_6$. It has a clear and strong Fano behavior, which is characteristic of the fingerprint of stage-1 graphite intercalation compounds.[24,27] When deintercalation was induced in the samples, a decrease of these $E_{2g}$ modes was remarkably observed [see Fig. 2(b)].

The fourth mode related to the $G$ line of their respective stage-2 compound is observed at 1612 $cm^{-1}$ for $KC_8$, 1600 $cm^{-1}$ for $LiC_6$, and at 1560 $cm^{-1}$ for $CaC_6$. The surprising low frequency in the case of $CaC_6$ was also found in Ref. 25 and explained as a deintercalated phase in $CaC_6$. As mentioned above, the increase of this fourth component is highlighted in the partly deintercalated stage-1 compounds in Fig. 2(b), and points toward a phase separation upon deintercalation.

### B. Analysis of the electron-phonon coupling

The previous results are very important for the correct determination of the stage, and electron-phonon coupling constant $\lambda_{ph}$ responsible for superconductivity within the BCS theory.[24,26,36] This constant is directly related to the intrinsic $G$-line phonon frequency, and to the adiabatic ($\omega_A$) and nonadiabatic ($\omega_{NA}$) phonon frequencies. Saitta *et al.*[26] have analyzed the EPC in many different stage-1 GICs from a difference in the experimental phonon frequency to the calculated phonon frequency in the adiabatic and nonadiabatic limit. In order to determine the electron-phonon scattering renormalized line width[24,26] $\gamma^{EPC}$ we used

$$\frac{\gamma^{EPC}}{2} = \sqrt{(\omega_{ph} - \omega_A)(\omega_{NA} - \omega_{ph})}. \quad (1)$$

We obtain $\gamma^{EPC}$ values for $KC_8$, $CaC_6$, and $LiC_6$, which are in very good agreement to our experimental $\Gamma_{ph}$ value obtained from our BWF fit (Table II). In Fig. 3 we show the location of our $\gamma^{EPC}$ with respect to the expected linear tendency to $\Gamma_{ph}$ as predicted by Saitta *et al.*[26] It is important to notice that some components of the $G$ line in $KC_8$, $CaC_6$, and $LiC_6$ bring a $\gamma^{EPC} = 0$, which means that they do not show the nonadiabatic effects for layered metals and therefore they do not contribute to the electron-phonon coupling constant $\lambda_{ph}$. In comparison to the experimental $\Gamma^{exp}$ and $\gamma^{EPC}$ from Refs. 23,37, and 38 [Fig. 3 (★)], our results using the $E_{2g_2}$ mode are in better agreement to the linear trend expected for $\Gamma \approx \gamma^{EPC}$. This confirms the importance of every optical mode in the range between the adiabatic and nonadiabatic frequency range ($\omega_A$–$\omega_{NA}$), and confirms that the $E_{2g_2}$ component is the intrinsic stage-1 vibrational mode with the strongest nonadiabatic effect on the EPC.

We now turn to a detailed analysis of the EPC constant $\lambda_{ph}$. Different values have been already reported and used to calculate the critical temperature of $KC_8$, $CaC_6$, and $LiC_6$ with values around 5 K, 11.5 K, and 0.9 K, respectively, in agreement with some experimental and theoretical studies.[8,40]

TABLE II. Electron-phonon coupling parameters from the $G$-line Raman analysis. The values of $\omega_{ph}$, $\Gamma_{ph}$, $\gamma^{EPC}$ are in $cm^{-1}$ and they were extracted from the BWF analysis of the Raman spectrum. $D_{exp}$ is the electron-phonon coupling strength from Eq. (3) in (eV/Å).

| $KC_8$ | $\omega_{ph}$ | $\Gamma_{ph}$ | $\gamma^{EPC}$ | $\gamma^{EPC}$[a] | $D_{exp}$ | $OB$[b] | $\lambda_{K,\Gamma}$[c] |
|---|---|---|---|---|---|---|---|
| **D** | 1274 | 24.3 | 230 | – | 14 | $K$ | 0.024 |
| $E_{2g_2}$ | 1510 | 125.6 | 163 | 157 | 51 | $\Gamma$ | 0.020 |
| $E_{2g_1}$ | 1547 | 70.9 | 0 | – | 36 | $\Gamma$ | – |
| $\lambda_{ph}$ | | | | | | | 0.044 |
| $CaC_6$ | $\omega_{ph}$ | $\Gamma_{ph}$ | $\gamma^{EPC}$ | $\gamma^{EPC}$[a] | $D_{exp}$ | $OB$[b] | $\lambda_{K,\Gamma}$[c] |
| **D** | 1358 | 24.3 | 0 | – | 14 | $K$ | 0.022 |
| $E_{2g_2}$ | 1510 | 71.0 | 68 | 68 | 36 | $\Gamma$ | 0.020 |
| $E_{2g_1}$ | 1525 | 70.9 | 34 | 36 | 36 | $\Gamma$ | 0.019 |
| $\lambda_{ph}$ | | | | | | | 0.061 |
| $LiC_6$ | $\omega_{ph}$ | $\Gamma_{ph}$ | $\gamma^{EPC}$ | $\gamma^{EPC}$[a] | $D_{exp}$ | $OB$[b] | $\lambda_{K,\Gamma}$[c] |
| **D** | 1364 | 24.3 | 43 | – | 14 | $K$ | 0.022 |
| $E_{2g_2}$ | 1546 | 71.0 | 157 | – | 36 | $\Gamma$ | 0.019 |
| $E_{2g_1}$ | 1585 | 70.9 | 0 | 0 | 36 | $\Gamma$ | – |
| $\lambda_{ph}$ | | | | | | | 0.041 |

[a]Calculated phonon full line width at half maximum due to phonon decay in dressed electron-hole pairs $\gamma_\sigma^{EPC}$ (Ref. 26).
[b]Optical branch assignment based in Refs. 8 and 39.
[c]Electron-phonon coupling constant from Eq. (2).

In order to extract $\lambda_{ph}$ from the phonon line width ($\Gamma$) and position ($\omega_{ph}$) from our Raman data we used[41]

$$\lambda_{\Gamma,K} = \frac{A_{uc}\, F_{\Gamma,K}^2}{2\, M\, \omega_{\Gamma,K}\, v_F^2}, \quad (2)$$

where the electron-phonon coupling strength is given by $D_{exp}$

$$\Delta\Gamma_G = \frac{A_{uc}\, D_{exp}^2}{8\, M\, v_F^2} \quad (3)$$

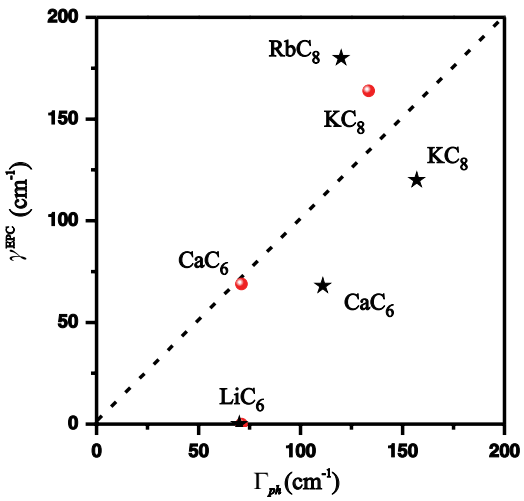


FIG. 3. (Color online) Calculated $\gamma^{EPC}$ [Eq. (1)] for different GICs as function of their width $\Gamma_{ph}$. Black stars (★) correspond to experimental values from Refs. 23,37, and 38. The dashed line represents the approximation of $\Gamma_{ph} \approx \gamma^{EPC}$. The red dots show our calculated EPC, which are in better agreement to the expected approximation to the $\Gamma_{ph}$ values.

and $A_{uc}$ is defined as the area of the graphene unit cell, $M$ is the carbon atom mass, $v_F$ is the Fermi velocity, $\Delta\Gamma_G$ is the Landau damping phonon decay rate given by $\Delta\Gamma_G = \Gamma_{\rm ph} - \Gamma_{\rm Graphite}$, and $F^2_{\Gamma,K}$ has dimensionality of a force taking into consideration the lattice displacement along the corresponding optical phonon mode. By using Eq. (2) and the definition of $F^2_\Gamma = 4\langle D^2_\Gamma\rangle_F$, and $F^2_K = 2\langle D^2_K\rangle_F$ from Refs. 39,41 we calculate the values for $\lambda_{\Gamma,K}$ for each phonon in the $\Gamma$-$K$ branch observed in the $G$-line region as summarized in the right column of Table II. $\langle D^2_{\Gamma,K}\rangle_F$ were taken from the DFT$_{\rm GGA}$ calculations in graphite[39] as they are closer to our electron-phonon coupling strength ($D_{\rm exp}$).

By using the averaged electron-phonon coupling constant $\lambda_{\rm ph} = \lambda_\Gamma + \lambda_K$, and the position $\omega_{\rm ph}$ from the strongest optical mode in $KC_8$, $CaC_6$, and $LiC_6$ one can estimate the critical temperature $T_c$ using McMillan's formula.[42] Taking our $\omega_{\rm ph}$ values converted into phonon temperature $\Theta$, $\mu^* \approx 0.14$ from Ref. 43 and $\lambda_{\rm ph}$ from the Raman analysis, we obtain $\lambda_{\rm ph} < 0.06$ values, which are too low to explain superconductivity within EPC mechanism using these high-frequency Raman active modes.

However, this is not a general behavior in intercalation compounds. Electron-phonon studies in alkali-intercalated fullerenes showed the possibility to attribute the strongest $\lambda_{\rm ph}$ contribution for superconductivity to the Hg(1) mode in $A_3C_{60}$ fullerides.[15,16] Moreover, in agreement to the analysis reported by Yao *et al*. in Ref. 16 our $D_{\rm exp}$ presented the same trend as the one observed in fullerides intercalation compounds. Therefore, we can confirm that the larger the value of $1/\mathbf{q}$, the weaker the coupling strength $D_{\rm exp}$ in GICs and fullerides.

On the other hand, in comparison to the EPC constant $\lambda_{\rm ARPES}$ reported using an analysis of the self-energy results in ARPES,[8,44] our $\lambda_{\rm ph}$ values are about a factor of 10–15 lower. Since, in the case of $CaC_6$ superconductivity was confirmed at $T_c = 11.5$ K, only the $\lambda_{\rm ARPES}$[44] would be sufficient to explain this high superconducting transition temperature. Hence, the low $\lambda_{\rm ph}$ proves that optical modes from the $G$ line in stage-1 GICs are not sufficient to explain $T_c$ in the electron-phonon-driven superconducting coupling mechanism and additional not optically active modes might play an important role.

## IV. CONCLUSION

We have performed a detailed *in situ* Raman study of the most common GICs ($KC_8$, $CaC_6$, and $LiC_6$). We identify four main peaks in the $D$- to $G$-band region, and all these Raman responses match the spread of different line shapes reported in the literature so far. From an evaluation of the fine structure in the $G$-line response we assign each peak to its corresponding vibrational mode and phonon branch.

We found the strongest Fano behavior of the $G$ line at 1510 cm$^{-1}$ in $KC_8$ and $CaC_6$, not like in $LiC_6$, which highlights the importance of this mode to the superconductivity coupling mechanism within the BCS theory, and confirms the importance of this $E_{2g_2}$ mode to nonadiabatic effects. By using this mode, we obtain a very good agreement to the theoretical predicted line width $\gamma^{\rm EPC} \simeq \Gamma_{\rm ph}$ especially for $CaC_6$.

Finally, we find a very small EPC $\lambda_{\rm ph} < 0.06$, which is much too low to explain the high $T_c$ in these graphite intercalated compounds. This points out that other phonons including acoustic modes and other electronic states might play an important role in explaining the superconducting pairing in GICs.

## ACKNOWLEDGMENTS

We acknowledge for the financial support of Project No. FWF-I377-N16, the OEAD AMADEUS PROGRAM financing, and the comments from Hidetsugu Shiozawa and Christian Kramberger. A.G. and M.J.R. thank the Engineering and Physical Sciences Research Council for funding.

*julio.chacon@univie.ac.at
†http://epm.univie.ac.at

[1] M. S. Dresselhaus and G. Dresselhaus, Adv. Phys. **30**, 139 (1981).
[2] A. Jorio, G. Dresselhaus, and M. S. Dresselhaus, Carbon Nanotubes, Advanced Topics in the Synthesis, Structure, Properties and Applications (2008).
[3] O. Gunnarsson, Rev. Mod. Phys. **69**, 575 (1997).
[4] A. H. Castro Neto, F. Guinea, N. M. R. Peres, K. S. Novoselov, and A. K. Geim, Rev. Mod. Phys. **81**, 109 (2009).
[5] G. Hennig and L. Meyer, Phys. Rev. **87**, 439 (1952).
[6] N. B. Hannay, T. H. Geballe, B. T. Matthias, K. Andres, P. Schmidt, and D. Macnair, Phys. Rev. Lett. **14**, 225 (1965).
[7] M. Kobayashi and I. Tsujikawa, J. Phys. Soc. Jpn. **46**, 1945 (1979).
[8] A. Gruneis, C. Attaccalite, A. Rubio, D. V. Vyalikh, S. L. Molodtsov, J. Fink, R. Follath, W. Eberhardt, B. Buchner, and T. Pichler, Phys. Rev. B **79**, 205106 (2009).
[9] M. Calandra and F. Mauri, Phys. Rev. Lett. **95**, 237002 (2005).
[10] R. M. Fleming, A. P. Ramirez, M. J. Rosseinsky, D. W. Murphy, R. C. Haddon, S. M. Zahurak, and A. V. Makhija, Nature (London) **352**, 787 (1991).
[11] A. F. Hebard, M. J. Rosseinsky, R. C. Haddon, D. W. Murphy, S. H. Glarum, T. T. M. Palstra, A. P. Ramirez, and A. R. Kortan, Nature (London) **350**, 600 (1991).
[12] M. J. Rosseinsky, A. P. Ramirez, S. H. Glarum, D. W. Murphy, R. C. Haddon, A. F. Hebard, T. T. M. Palstra, A. R. Kortan, S. M. Zahurak, and A. V. Makhija, Phys. Rev. Lett. **66**, 2830 (1991).
[13] A. Y. Ganin, Y. Takabayashi, Y. Z. Khimyak, S. Margadonna, A. Tamai, M. J. Rosseinsky, and K. Prassides, Nature Mater. **7**, 367 (2008).
[14] M. Capone, M. Fabrizio, C. Castellani, and E. Tosatti, Rev. Mod. Phys. **81**, 943 (2009).
[15] J. Winter and H. Kuzmany, Phys. Rev. B **53**, 655 (1996).
[16] M. Yao, V. Pischedda, and A. San Miguel, J. Phys.: Condens. Matter **23**, 115701 (2011).
[17] C. M. Varma, J. Zaanen, and K. Raghavachari, Science **254**, 989 (1991).

[18]M. Schlüter, M. Lannoo, M. Needels, G. A. Baraff, and D. Tomanek, J. Phys. Chem. Solids **53**, 1473 (1992).
[19]T. E. Weller, M. Ellerby, S. S. Saxena, R. P. Smith, and N. T. Skipper, Nature Phys. **1**, 39 (2005).
[20]J. S. Kim, R. K. Kremer, L. Boeri, and F. S. Razavi, Phys. Rev. Lett. **96**, 217002 (2006).
[21]D. G. Hinks, D. Rosenmann, H. Claus, M. S. Bailey, and J. D. Jorgensen, Phys. Rev. B **75**, 014509 (2007).
[22]I. I. Mazin, L. Boeri, O. V. Dolgov, A. A. Golubov, G. B. Bachelet, M. Giantomassi, and O. K. Andersen, Physica C **460**, 116 (2007).
[23]J. Hlinka, I. Gregora, J. Pokorny, C. Herold, N. Emery, J. F. Mareche, and P. Lagrange, Phys. Rev. B **76**, 144512 (2007).
[24]M. P. M. Dean, C. A. Howard, S. S. Saxena, and M. Ellerby, Phys. Rev. B **81**, 045405 (2010).
[25]A. Mialitsin, J. S. Kim, R. K. Kremer, and G. Blumberg, Phys. Rev. B **79**, 064503 (2009).
[26]A. M. Saitta, M. Lazzeri, M. Calandra, and F. Mauri, Phys. Rev. Lett. **100**, 226401 (2008).
[27]J. C. Chacón-Torres and T. Pichler, Phys. Status Solidi B **248**, 2744 (2011).
[28]S. A. Solin and N. Caswell, J. Raman Spectrosc. **10**, 129 (1981).
[29]N. Emery, C. Herold, M. d'Astuto, V. Garcia, C. Bellin, J. F. Mareche, P. Lagrange, and G. Loupias, Phys. Rev. Lett. **95**, 087003 (2005).
[30]R. J. Nemanich, S. A. Solin, and D. Guerard, Phys. Rev. B **16**, 2965 (1977).
[31]G. L. Doll, P. C. Eklund, and J. E. Fischer, Phys. Rev. B **36**, 4940 (1987)
[32]C. A. Howard, M. P. M. Dean, and F. Withers, Phys. Rev. B **84**, 241404 (2011).
[33]P. C. Eklund and K. R. Subbaswamy, Phys. Rev. B **20**, 5157 (1979).
[34]F. Tuinstra and J. L. Koenig, J. Chem. Phys. **53**, 1126 (1970).
[35]A. C. Ferrari and J. Robertson, Phys. Rev. B **61**, 14095 (2000).
[36]L. Pietronero and S. Strässler, Europhys. Lett. **18**, 627 (1992).
[37]D. Guerard and A. Herold, Carbon **13**, 337 (1975).
[38]G. L. Doll, M. H. Yang, and P. C. Eklund, Phys. Rev. B **35**, 9790 (1987).
[39]M. Lazzeri, C. Attaccalite, L. Wirtz, and F. Mauri, Phys. Rev. B **78**, 081406 (2008).
[40]G. Profeta, M. Calandra, and F. Mauri, Nature Phys. **8**, 1 (2012).
[41]D. M. Basko, S. Piscanec, and A. C. Ferrari, Phys. Rev. B **80**, 165413 (2009).
[42]M. Schlüter, M. Lannoo, M. Needels, G. A. Baraff, and D. Tomanek, Phys. Rev. Lett. **68**, 526 (1992).
[43]W. L. McMillan, Phys. Rev. **167**, 331 (1968).
[44]T. Valla and Z. Pan, *Physics and Applications of Graphene* (InTech, Rijeka, Croatia, 2011).